sustainability

MDPI

Article

A Sustainable Graphene Based Cement Composite

Sardar Kashif Ur Rehman [1,*], Zainah Ibrahim [1,*], Shazim Ali Memon [2,*], Muhammad Faisal Javed [1,3] and Rao Arsalan Khushnood [4]

[1] Department of Civil Engineering, University of Malaya, 50603 Kuala Lumpur, Malaysia; arbabf1@gmail.com
[2] Department of Civil Engineering, School of Engineering, Nazarbayev University, 010000 Astana, Kazakhstan
[3] Department of Civil Engineering, COMSATS Institute of Information Technology, 22060 Abbottabad, Pakistan
[4] NUST Institute of Civil Engineering, School of Civil and Environmental Engineering, National University of Sciences and Technology, 44000 Islamabad, Pakistan; arsalan.khushnood@nice.nust.edu.pk
* Correspondence: kashif@engineersdaily.com (S.K.U.R.); zainah@um.edu.my (Z.I.); shazim.memon@nu.edu.kz (S.A.M.)

Received: 2 May 2017; Accepted: 4 July 2017; Published: 13 July 2017

Abstract: The rheological properties of fresh cement paste with different content of graphene nanoplatelets (GNPs), different shear rate cycles and resting time was investigated. The rheological data were fitted by the Bingham model, Modified Bingham model, Herschel–Bulkley model and Casson model to estimate the yield stress and plastic viscosity, and to see trend of the flow curves. The effectiveness of these rheological models was expressed by the standard error. Test results showed that yield stress and plastic viscosity increased with the increase in the content of graphene in the cement based composite and resting time while the values of these parameters decreased for higher shear rate cycle. In comparison to control sample, the GNP cement based composite showed 30% increase in load carrying capacity and 73% increase in overall failure strain. Piezo-resistive characteristics of GNP were employed to evaluate the self-sensing composite material. It was found that, at maximum compressive load, the electrical resistivity value reduced by 42% and hence GNP cement based composite can be used to detect the damages in concrete. Finally, the practical application of this composite material was evaluated by testing full length reinforced concrete beam. It was found that graphene–cement composite specimen successfully predicted the response against cracks propagation and hence can be used as self-sensing composite material.

Keywords: rheological properties; self-sensing; piezo-resistivity; graphene nanoplatelets; structural health monitoring

1. Introduction

Concrete is the most widely used construction material and usually placed in the plastic form. Fluidity, homogeneity, consistency and workability are the key elements that greatly depend on viscosity of concrete and need to be considered during the mixing and placing of concrete. Any shortcoming in these parameters will lead to bleeding, segregation, laitance and cracking of the concrete [1]. Therefore, the rheological properties of concrete are of utmost significance to achieve homogeneity and good workability and have a strong influence on the overall fresh properties of the concrete [2]. With the advancement in nanotechnology, researchers are emphasizing more on the effect of nanomaterials on cement composite [3]. Numerous researchers studied the effect of various engineered nanomaterials on flow characteristics of the cement paste [4–6] and most of the research was focused on the rolled sheets of graphene and its derivatives, i.e., CNTs (carbon nanotubes) and graphene oxide [6–8]. However, the rheological properties of graphene cement paste remained unexplored and rarely reported. Therefore, an in-depth knowledge of the connection of graphene and

rheology of cement paste is required. The flow properties of the cement paste are usually acquired by shear stress and shear rate. Later from the flow curves, viscosity and other flow parameters are calculated by using mathematical models. These rheological models statistically determine the yield stress (shear stress at zero shear rate), plastic viscosity (generalized viscosity for a range of shear rate) and predict the specific trend of the flow. As, these mathematical models possess statistical errors; therefore, one model cannot predict accurately the deformation of cement paste [9]. Therefore, in this research, four rheological models were used to investigate the flow properties of the graphene cement based composite.

Graphene possesses some amazing and extraordinary properties such as huge specific surface area (2630 $m^2 \cdot g^{-1}$), high intrinsic strength (130 GPa), firm Young's module (~1.0 TPa) and high electrical transport properties [10]. Therefore, incorporation of graphene in cement composite will not only alter the rheological characteristics but also affect the electrical properties of the composite. The electrical properties of the GNP–cement composite are important and can be used to monitor the damage in a concrete structure for the purpose of maintaining safe, reliable and sustainable civil infrastructure. It is known that non-destructive test offers skills for speedily and effectively monitoring these structures [11,12]. However, Self-sensing concrete, which can monitor its own strain, is the need of this era. The cement based composite reinforced with conducting fillers can observe its own strain by monitoring the changes in the electrical resistivity values [12]. Self-sensing ability is related to the breaking of conducting fibers when cracks are initiating in the cement based composite consequently enhancing the resistivity of the overall sample. If cracks are opening up due to tensile or fracture loading then resistivity values will be positive while it will be negative when subjected to compressive loading. Newly developed engineering nanocarbons are capable of fabricating new kind of high-performance tailored multifunctional cement-based composite that is capable of self-sensing the real-time damage [13–16]. Carbon nanotubes (CNTs) are composed of sp^2 hybridized carbon atoms, sheets of single layered graphene sheet rolled up in a cylindrical tube [17]. If these rolled sheets of CNTs are opened up in one plane, then it forms the two-dimensional sheet-like structure. These two-dimensional sheets, i.e., graphene nanoplatelets (GNPs) have even greater surface area and aspect ratio. Sixuan [18] investigated the effect of crack depth of the GNP reinforced mortar on the change in the electrical resistance. It was revealed that the specimens (cube and prism shapes) responded to an increase in electrical resistance as the depth of crack became larger. For the same relative crack depth, the change in electrical resistance for the cube was more significant as compared to that of the prism. However, as per authors' knowledge, the response of the GNP–cement composite to various damage levels has not been investigated.

Therefore, in this study, the flow properties of the GNP cement paste were investigated by using Bingham, Modified Bingham, Herschel–Bulkley and Casson models. Variation in flow curves of cement paste with different percentages of graphene nanoplatelets was determined. Rheological properties of graphene cement paste with various resting time (time between sample preparations to casting) and shear rate cycles were also evaluated. Later, the self-sensing properties of the GNP-based cementitious material were determined. The four-probe method was used for electrical resistance measurement purpose. Strain-sensing and fractional change in resistance were observed and used for determining self-sensing characteristics. Finally, application of GNP–cement composite specimen was evaluated on the reinforced beam.

2. Rheological Models

The rheological properties of the cement paste are directly related to the workability, flowability and consistency of the concrete. Cement paste has the complex rheological behavior as it depends on several parameters like water cement ratio, chemical admixtures, shear rate and supplementary cementitious materials [19]. The rheological models consider several factors which have great influence on cement paste rheology, and are necessary to be considered to achieve better and realistic approaches. Due to the influence of several factors in the rheological model for cement paste, the flow behavior

cannot be predicted with best fitting curves by using single model [20]. It is also known that the accuracy and efficiency of the mathematical model depend on absolutely fitting the experimental data. Hence, four rheological models have been selected from various standards and researchers [9].

$$\text{Bingham Model} \quad \tau = \tau o + \mu p \ddot{Y} \tag{1}$$

$$\text{Modified Bingham Model} \quad \tau = \tau o + \mu p \ddot{Y} + c\ddot{Y}^2 \tag{2}$$

$$\text{Herschel-Bulkley Model} \quad \tau = \tau o + K\ddot{Y}^n \tag{3}$$

$$\text{Casson Model} \quad \sqrt{\tau} = \sqrt{\tau o} + \sqrt{\mu p} \cdot \sqrt{\ddot{Y}} \tag{4}$$

In these models, τ is considered as shear stress, τ_o as yield shear stress, μ_p as plastic viscosity, $\ddot{Y}$ as shear rate, K as consistency, n as power rate index and c as regression constant.

Bingham model has been most widely used by researchers to determine the yield stress and plastic viscosity of the cement paste [21]. Bingham mathematical equation is linear (Equation (1)) and comparatively convenient to use for an analytical solution [22]. However, it fails to fit into the nonlinear portion of the flow curve at low shear rate and cannot predict yield shear stress accurately especially for shear thickening behavior [20]. To overcome this deficiency, the Bingham equation was modified and was used to fit the model in pseudo-plastic or shear thickening behavior. The mathematical expression of the modified Bingham model is given by Equation (2) [7]. However, it restricts the response of the cement paste to second order polynomial. Shear thickening behavior of the cement paste was further quantified by using Herschel–Bulkley model. This model has the characteristics of both Bingham and Power models and is given by Equation (3) [22]. This model is based on power rate index (n), which can predict the shear thinning and shear thickening behavior of the cement paste. With the increase in power rate index (n) value more than 1, the shear thickening behavior of the paste will be more prominent. The Casson model has two adjustable parameters, i.e., yield shear stress and plastic viscosity (Equation (4)). It uses the square root of these values, which makes its relation complex and difficult to explain. According to [19], it can predict the viscosity at a very high shear rate (infinite shear rate). However, this equation has a limitation in predicting the flow parameters for very concentrated suspensions [19]. As per [23] observation, Casson equation fits very well to various types of fluid and is more appropriate to use when compared with Herschel–Bulkley equation, yet, it is difficult to explain in most cases.

The ability of any analytical model to accurately match the nonlinear regression at low shear rate will define its accuracy. As this ability varies with each mathematical expression, therefore, the calculated rheological parameters especially yield stress values can offer different values for different models. Standard error for each rheological model has been determined using Equation (5). It depends on the normalized standard deviation. Finally, a comparison has been drawn amongst the calculated values to determine the effective and best-fitted model.

$$Standard\ error = \frac{1000 * \left\{ \frac{\sum (measured\ value - calculated\ value)^2}{(number\ of\ data\ points - 2)} \right\}^{1/2}}{(Maximum\ measured\ value - Minimum\ measured\ value)} \tag{5}$$

3. Experimental Methodology

3.1. Materials

Ordinary Portland cement (Tasek Corporation Berhad) CEM I 42.5N (Type I) which was based on MS EN 197-1 having specific gravity 3.14 and Blaine surface area 0.351 (m^2/g) was used. The properties of GNP, purchased from Graphene Laboratories, Inc. USA are enlisted in Table 1. Deionized water was used for making cement based composite.

Table 1. The properties of GNPs used for this experiment.

Property	Description/value
Average Flake Thickness (nm)	12 (30–50 Monolayers)
Average particle (lateral) size (nm)	~4500 (1500–10,000 nm)
Specific surface area, SSA (m^2/g)	80
Purity	99.2%
Color	Black

3.2. Preparation of Samples

For specimen's preparation cement, GNP and deionized water were used. The details of mix proportions are given in Table 2. Here, M0 represents the control sample of cement paste while GM3, GM5 and GM10 represent samples containing 0.03%, 0.05% and 0.10% GNP by weight of cement, respectively. The GNP samples (GM3, GM5 and GM10) were used to study the influence of graphene on rheological characteristics of cement paste while for determining the strain-sensing characteristics of graphene–cement based composite, only GM3 having least percentage of GNP was considered. All measurements were repeated with identical samples for three times and averaged. For sample preparation, firstly, GNP (by weight of the cement) was added to the deionized water. To exfoliate nanoparticles, the sample was ultrasonicated (Fisher Scientific™ Model 505 Sonic Dismembrator) for 3 min followed by magnetic stirring for 1 h to ensure uniform dispersion of GNP. Thereafter, cement was added to this aqueous solution of GNP and mixed thoroughly for 5 min in spar mixer (SP-800A). Initially, the speed of the mixer was kept low for 2 min then static for 10 s and finally high for another 2 min. Finally, rheological characteristics of cement paste were measured. The workability of cement paste was determined by ASTM C 1437-15 [24] while for determining electrical properties, prism having dimensions of 160 × 40 × 40 mm was casted. Four-stainless-steel wire meshes (11 × 11 mm cross section) with an average thickness of 1.3 mm and dimensions of 40 × 70 mm was inserted in the samples to measure the electrical properties as shown in Figure 1a. The outer two wire meshes were positioned at 10 mm from the ends of the prism while the inner two wire meshes were positioned at 40 mm from the outer wire mesh. The detailed dimensions are given in Figure 1a. The surface morphology of GNP–cement composite was investigated using Field emission scanning electron microscope (FE-SEM, AJSM-7600F with semi-in-lens) while the elemental composition was acquired using FESEM coupled with an energy dispersive X-ray spectrometer (EDS).

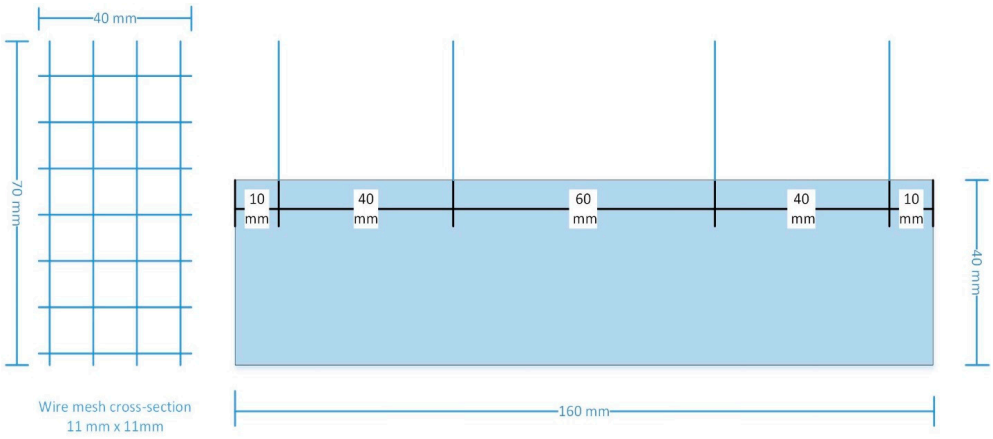

(**a**)

Figure 1. *Cont.*

Figure 1. Description of specimen and test setup (**a**) Dimensions of graphene–cement composite specimen with wire mesh details; (**b**) placement of specimen on reinforcement; (**c**) casting of reinforced concrete (RC) beam; and (**d**) overall test setup for measuring the electrical properties of graphene–cement composite specimen in the RC beam.

Table 2. Mix Proportions.

Mix Design	W/C Ratio	Cement (g)	Water (mL)	GNP (mg)	GNP/Cement (%)
M0	0.4	100	40	0	0
GM3	0.4	100	40	30	0.03
GM5	0.4	100	40	50	0.05
GM10	0.4	100	40	100	0.10

3.3. Rheological Measurements

The rheological properties were characterized by using Rheometer MCR302 (Anton-Paar) while Rheoplus software was used to monitor and analyze the data points. To determine the rheological characteristics of the GNP–cement paste, smooth parallel plates with a gap thickness of 0.6 mm were used. At first, approximately 15 mL of GNP–cement paste was added on the plate having diameter 25 mm at a fixed temperature of 25 °C. The cement paste was held at rest and after 10 min it was pre-sheared at a shear rate of 100 s^{-1} for 60 s. This was done to re-homogenize the sample, as cement paste has thixotropic character [25]. Then, after 5 min, shear rate was applied from 0.6 s^{-1} to 100 s^{-1} and then back from 100 s^{-1} to 0.06 s^{-1} in 20 decreasing steps. The downslope curve data was used for calculation of rheological parameters. Similarly, GNP–cement paste was also run for two different shear rates cycles, i.e., from 200 s^{-1}–0.6 s^{-1} with 40 steps and 300 s^{-1}–0.6 s^{-1} with 60 steps. The flow

properties were also determined at different time interval, i.e., 0 min, 30 min and 60 min. For 30 and 60 min resting time, the samples were manually stirred for 15 s before measuring the rheological data. It is pertinent to mention here that the effect of graphene and its content on the rheology of cement paste was investigated by using mix M0, GM3, GM5 and GM10, while to examine the influence of different shear rate cycle range (100–0.6 s^{-1}, 200–06 s^{-1} and 300–0.6 s^{-1} represented by symbols a, b and c respectively) and different resting times (0, 30 and 60 min time between sample preparation and casting) on rheological properties, only M0 and GM3 mix were used. The detailed description about the shear rate cycle range and resting time of various samples for measuring rheological data is given in Table 3. All measurements were repeated with identical samples for three times and averaged. The apparent viscosity, shear stress and shear rate of GNP–cement paste with different proportions were measured by the rheometer while the yield stress and plastic viscosity of the GNP–cement paste was determined by using the Bingham, Modified Bingham, Herschel–Bulkley and Casson models.

Table 3. Description of rheological samples.

Sample	Sher Rate Cycle Range (s^{-1})	Resting Time (min)
Effect of graphene percentage		
M0 (Control)	200–0.6	0
GM3	200–0.6	0
GM5	200–0.6	0
GM10	200–0.6	0
Effect of shear rate cycle		
M0a	100–0.6	0
M0b	200–0.6	0
M0c	300–0.6	0
GM3a	100–0.6	0
GM3b	200–0.6	0
GM3c	300–0.6	0
Effect of resting time		
M0–0	200–0.6	0
M0–30	200–0.6	30
M0–60	200–0.6	60
GM3–0	200–0.6	0
GM3–30	200–0.6	30
GM3–60	200–0.6	60

3.4. Test Setup for Electrical Properties

The four-probe method was used to determine the piezo-resistive properties of the GNP–cement composite specimens. Four-probe method involves four electrical contact points in which voltage is measured through the inner two electrical contacts while the current is measured using outer two electrical contacts. [26] Four-probe method is better than the two- probe method because measured resistance does not include the contact resistance [27]. According to Han et al. [27], the space between the current pole and voltage pole is very important. However, its influence is marginal if space is more than 7.5 mm. Various researchers used different spacing in their experimental work. Li et al. [28] used the spacing of 10 mm while Le et al. [29] used 40 mm spacing between current and voltage measuring probes. Similarly, the distance between the two voltage measuring probes is not fixed and its value varies. Li et al. [28] used the 40 mm gap between two measuring probes while Le et al. [29] used 80 mm gap. As resistivity values remain unaffected provided that the spacing is above threshold value [27], in this research, we used 40 mm spacing between the current measuring probe and voltage measuring probes and 60 mm between two voltage measuring probes. Pang et al. [30] explored the effect of percentage of graphene nanoplatelets on the strain and damage sensing of the composites. They found that with increase in the percentage of graphene nanoplatelets in cement based composite,

the fractional change in resistance values was also increasing. Therefore, based on the study of Pang et al. [30], only M0 and GM3 specimens were considered to explore the electric resistivity of cement based composite materials.

The setup for measuring the electrical resistivity consist of Instron 600 kN machine used for applying a compressive load, TDS-530 data logger to record the voltage measurements, a DC power supply and 10-ohm resistance. Specimens were placed in Instron machine and a constant voltage of 15 V through DC power supply was applied to the samples (Figure 1a). Inner wire meshes were connected to the data logger and measures the voltage drop in V. Meanwhile, one of the outer wire meshes was connected to the negative terminal of the power supply and the remaining outer wire mesh was connected to the resistor followed by the connection to the second channel of the data logger and positive terminal of the power supply forming a series circuit. Finally, the practical application of these GNP–cement composite specimen was investigated by testing the reinforced concrete (RC) beam having cross-sectional dimension 200 × 300 (mm) and span length 3200 mm. For this purpose, GM3 specimen was placed inside the beam in center at the time of beam casting as shown in Figure 1b,c. The beam was tested under flexural loading using Instron 600 kN and response of the GNP–cement composite specimen was recorded using 15 V DC power supply and TDS 530 data logger. The test setup is shown in Figure 2c.

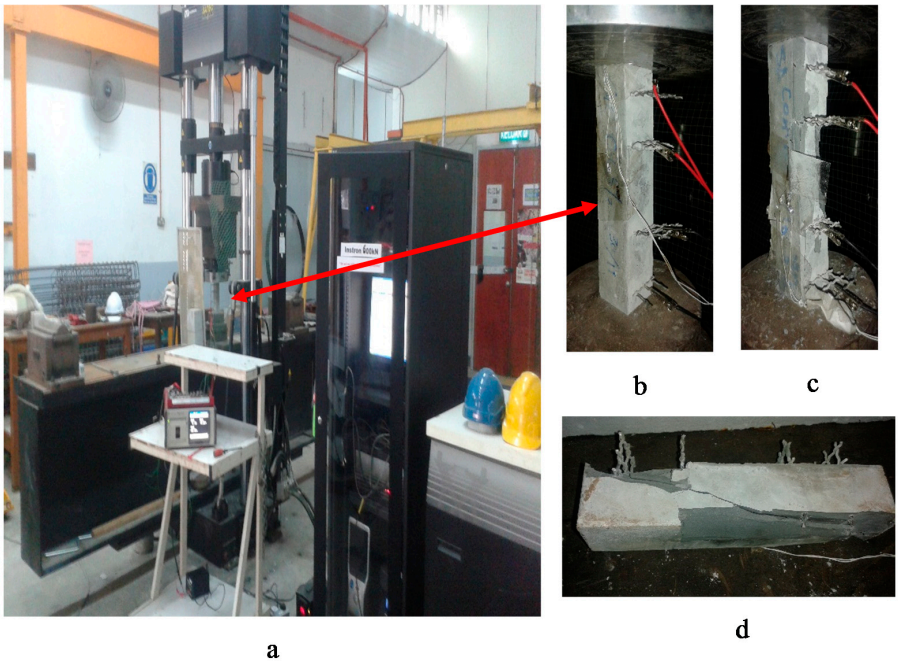

Figure 2. Measurement of electrical properties (**a**) The overall set up for the four-probe method for the electrical properties testing; (**b**) placing of the specimen into the Instron 600 kN machine; (**c**) sample failure under compression; and (**d**) propagation of cracks in failed sample.

4. Results and Discussion

4.1. Rheological Characteristics of GNP–Cement Composite

Variation in rheological characteristics of both cement paste and graphene–cement paste were observed, which originates due to mix composition of the paste, shear rate cycle, resting time and rheological model. As these rheological methods determine the flow property values from statistical trials, several values can be obtained. However, in this research, best curve fitting and minimizing the standard error was considered in determining the rheological flow values. The effect of mix composition mainly includes water to cement ratio, admixture, mixing and testing technique [31]. As these parameters were studied in detail [9,31], all these factors were kept constant and only effect

of graphene/cement ratio, shear rate range, and resting time was investigated. Moreover, the parallel plates, whose results are close to reality, were used to determine the rheological characteristics of cement based composites [2]. However, particle sedimentation or "creaming" occurs more in the parallel plate, which may contribute to increase the viscosity [32].

4.1.1. Yield Stress

Yield stress values were determined by Bingham model, Modified Bingham model, Herschel–Bulkley (HB) model and Casson model. The results are presented in Table 4. Due to slippage effect and smooth surface of parallel plates, low yield stress values were found [9]. Generally, the values of yield stress obtained by modified Bingham model were highest followed by Bingham, HB and Casson model. For all rheological models, the values of yield stress increased with the increase in the percentage of graphene in the cement matrix. This increase in yield stress values is in line with the available literature on the derivatives of graphene. The increase in yield stress values for graphene–cement paste might be due to higher surface area of graphene due to which it requires more amount of water for lubrication of graphene [33]. Shang et al. [6] carried out experimental investigation to study the effect of graphene oxide on rheological properties of cement paste and found that in comparison to plain cement, the value of yield stress increased by approximately four times for 0.08% of graphene oxide cement paste. It was noticed that negatively charged graphene nanoplatelets in water interacted with cement particles by electrostatic interaction and formed flocs. Wang et al. [7] also detected the increase in flocculation structures having higher dosage of graphene oxide (GO) in cement paste. According to literature [6], these large agglomerates entrap some water molecules, which reduce the content of free available water. Therefore, it can be concluded that by keeping the water cement (w/c) ratio constant, the values of rheological parameters will increase.

Table 4. Yield stress values determined by various rheological models.

Sample	Bingham (Pa)	Modified BM (Pa)	HB (Pa)	Casson (Pa)
Effect of graphene percentage				
M0 (Control)	1.53	1.76	1.22	0.52
GM3	1.67	1.79	1.30	0.62
GM5	1.84	1.89	1.48	0.79
GM10	1.90	1.93	1.53	0.80
Effect of shear rate cycle				
M0a	1.60	1.83	1.27	0.55
M0b	1.53	1.76	1.22	0.52
M0c	1.46	1.46	1.17	0.45
GM3a	1.74	1.86	1.34	0.64
GM3b	1.67	1.79	1.30	0.62
GM3c	1.51	1.61	1.21	0.50
Effect of resting time				
M0-0	1.53	1.76	1.22	0.52
M0-30	1.65	1.85	1.38	1.75
M0-60	2.54	2.88	3.64	1.93
GM3-0	1.67	1.79	1.30	0.62
GM3-30	1.72	1.92	1.42	1.81
GM3-60	3.78	2.19	1.65	4.91

For the case of shear rate cycle, the values of yield stress decreased when the shear rate cycle increases from 100–0.6 s^{-1} to 300–0.6 s^{-1}. This is possibly due to destruction of potential agglomerated structures in cement paste. For high shear rate cycle, the resistance to flow was reduced and hence shear thinning behavior was dominant. Finally, for both control and GNP–cement paste, the yield stress values increased with the increase in resting time as shown in Table 4. The increase in rheological parameters may be attributed to: (a) hydration reaction of cement paste; and (b) presence of suspended particles (graphene).

4.1.2. Viscosity

Plastic viscosity represents the deformation of cement pastes due to external loading [7]. Plastic viscosities were calculated from the flow curve using the Bingham, Modified Bingham and Casson models. The results are presented in Figure 3. Generally, for control sample (M0), Bingham model showed the highest value of plastic viscosity followed by the Casson and Modified Bingham (Figure 3a). However, for the GM3 sample, Modified Bingham showed the highest value of plastic viscosities followed by the Casson and Bingham model (Figure 3a). Furthermore, direct relationship between graphene and plastic viscosity was observed, as plastic viscosity increased with the increase in the amount of graphene in cement composite. These results are in line with Shang et al. [6], who found that the plastic viscosity values increased by 78% with the addition of 0.04% graphene oxide in plain cement mix. When samples were subjected to high shear rate cycle, the plastic viscosity reduced as shown in Figure 3b. Shang et al. [6] reported that the apparent viscosities are dependent on the shear rate, i.e., at low shear rate, the values of apparent viscosities would be higher while at high shear rate, the values of viscosities would be lower. A possible reason for this may be due to the breaking of the agglomerates of cement paste which in turn resulted in lower apparent viscosity. It was noticed that the values of plastic viscosity increased with the increase in resting time as shown in Figure 3c. It might be related to the hydration of cement particles and the fractional resistance between cement and graphene sheets. The influence of hydration of cement particles and fractional resistance was dominant for the resting time of 60 min, in which plastic viscosity was very high.

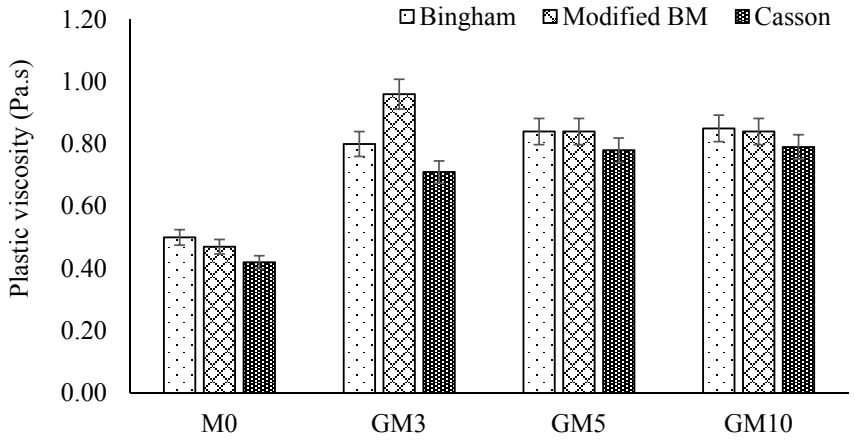

(**a**)

Figure 3. *Cont.*

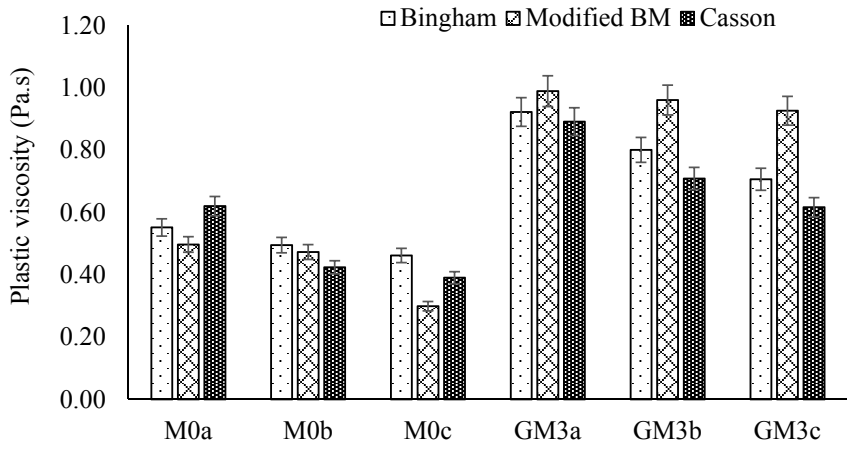

(**b**)

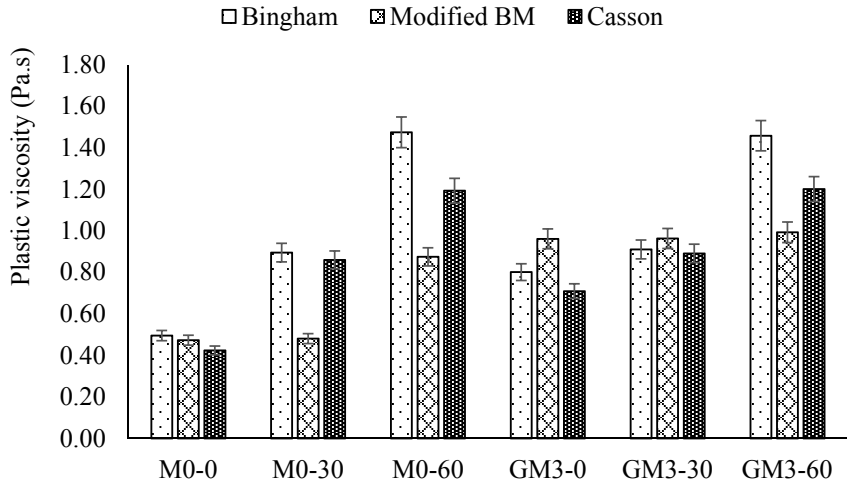

(**c**)

Figure 3. Plastic viscosity values (Pa.s) for different mixes calculated by Bingham, Modified Bingham and Casson models using smooth parallel plate: (**a**) effect of graphene percentage; (**b**) effect of shear rate cycle range; and (**c**) effect of resting time.

4.1.3. Consistency and Power Rate Index

The trend of the viscosity data was determined using Herschel–Bulkley (HB) model, which considers two factors, i.e., consistency (K) and the power rate index (n). By considering these factors, the relationship between viscosity trend and the shear rate of the flow curve can be determined [9]. Based on power rate index values "n", it also provides the information about the shear deformation, i.e., shear thickening ($n > 1$) or shear thinning ($n < 1$) [7] The consistency (K) has no physical meaning and difficult to compare because of its dimension ($Pa.s^n$) which is dependent on "n" [34]. Wang et al. [7] studied the shear deformation for graphene oxide in cement paste and found that cement paste curve can be divided into shear thinning and shear thickening stage based on the inflection point. They suggested that cement paste with higher graphene oxide content shows the shear thinning effect at high shear rates. The values of the consistency and power rate index for various samples are given in Table 5. It can be seen that the "n" values are less than one and hence cement paste behaves as shear thinning. However, for 60 min resting, the value of "n" for samples M0–60 and GM3-60 exceeded 1, indicating shear thickening behavior. When cement paste comes in contact with water then

coagulations and links are formed between two cement particles. With the increase in resting time, these links become strong and provide resistance to flow of cement paste [35]. Therefore, hydration reactions and presence of permanent links between cement particles will result in high resistance to flow.

Table 5. Consistency and rate index values calculated by Herschel–Bulkley model.

Sample	Consistency, K	Rate Index, n
Effect of graphene percentage		
M0 (Control)	0.60	0.96
GM3	0.97	0.97
GM5	0.99	0.98
GM10	0.97	0.98
Effect of shear rate cycle range		
M0a	0.51	0.90
M0b	0.60	0.96
M0c	0.29	0.60
GM3a	0.96	0.99
GM3b	0.97	0.97
GM3c	0.96	0.98
Effect of resting time		
M0–0	0.60	0.96
M0–30	0.96	0.98
M0–60	0.22	1.21
GM3–0	0.97	0.97
GM3–30	0.92	0.99
GM3–60	0.99	1.10

4.1.4. Standard Error

Standard error values for the various rheological models were calculated using Equation (5) and are given in Table 6. A lower value of standard error represents the best-fitting of the mathematical model to the flow curve. It was observed that HB model and Modified Bingham model showed less standard error while Bingham model and Casson model showed higher values of standard error. As HB and Modified Bingham models are nonlinear, they predicted the flow behavior more accurately. Bingham model has a linear mathematical relation and hence it showed higher standard error. Casson model has a limitation in predicting the concentrated suspension [19] and hence it is believed that it showed larger values of standard error. It was noted that, for M0c sample, all of the rheological models showed large values of standard error. It may be due to some calculation and experimental error regarding the flow curve data, as, for the same high shear rate cycle range, GM3c specimen showed comparatively low standard error values. GM10 mix showed the maximum standard error values for all mathematical models. As higher dosage of nanomaterials, i.e., graphene and graphene oxide, results in the formation of flocculation structures in cement paste [7]. Therefore, it is believed that the higher values of standard error may be due to the formation of these flocculated suspensions in the cement paste.

Table 6. Values of standard error for various rheological models.

Sample	Bingham	Modified BM	HB	Casson
Effect of graphene percentage				
M0 (Control)	74.53	74.39	74.39	73.63
GM3	89.01	34.29	70.54	82.93
GM5	30.58	30.67	45.07	57.29
GM10	233.26	223.55	261.57	283.10
Effect of shear rate cycle range				
M0a	163.63	244.69	280.44	140.10
M0b	74.53	74.39	74.39	73.63
M0c	344.36	285.05	319.14	318.37
GM3a	39.39	221.50	28.71	111.43
GM3b	89.01	34.29	70.54	82.93
GM3c	154.96	88.57	94.39	164.24
Effect of resting time				
M0-0	74.53	74.39	74.39	73.63
M0-30	117.72	65.26	123.06	111.40
M0-60	80.53	52.44	51.58	95.21
GM3-0	89.01	34.29	70.54	82.93
GM3-30	91.37	85.60	95.89	97.71
GM3-60	92.42	69.05	73.16	111.50

4.2. Fresh and Hardened Properties of GNP–Cement Composite

The results of workability test are presented in Table 7. The flow diameter of GM3 was found to be 8.5% less when compared to M0. Pan et al. [36] used 0.05% of graphene oxide in cement paste (w/c = 0.5) and observed 41.7% reduction in the slump diameter in comparison to control cement paste. Similarly, for 2% carbon nanotubes in cement paste (w/c = 0.5), 48.9% reduction in slump diameter was found in comparison to control cement paste [37]. Possible reason for reduction in flow diameter could be the large surface area of the graphene sheets, which require more amount of water for lubrication and in turn decrease the free available water. Therefore, the overall workability of the cement paste was reduced by addition of graphene in cement paste.

Table 7. Flow diameter, maximum compressive load and corresponding resistivity values.

Specimen	Flow Diameter (mm)	Maximum Compressive Load (kN)	Four Probe Resistivity at Maximum Compressive Loading (kΩ cm)
M0	175	61	32.93
GM3	160	80	19.12

Stress–strain curves for the M0 and GM3 are given in Figure 4. It can be seen that the addition of GNP greatly enhances the load carrying capacity of the cement paste (Table 7). The enhancement in compressive strength was about 30% as compared to mix M0. It was also observed that GM3 specimen showed more ductile behavior as compared to M0. The percentage strain produced in GM3 increased up to 73%, showing ductile nature of graphene–cement paste. The increase in compressive strength and strain may be attributed to the higher strength of graphene, template effect, and crack bridging by graphene sheets [38]. These results are in agreement with the study of Pan et al. [36] performed on graphene oxide based cement composites. For cement paste containing 0.05% graphene oxide, an improvement of about 22% in compressive strength was observed when compared to control specimen.

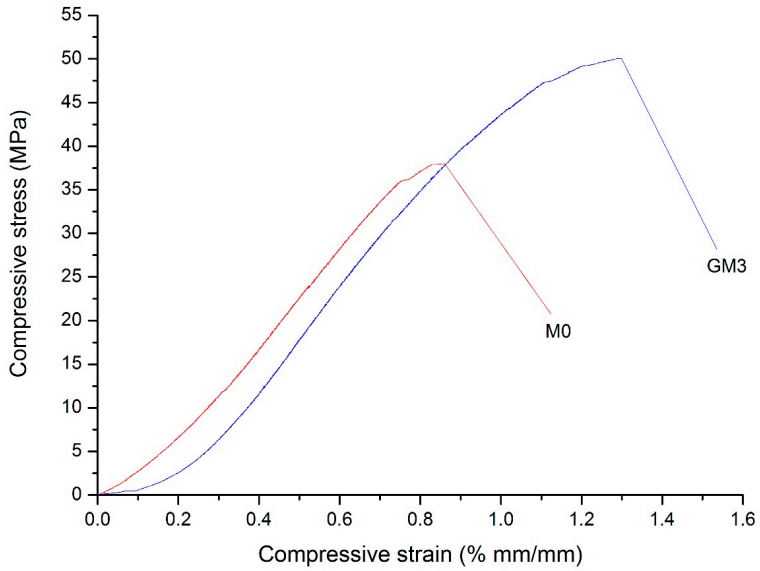

Figure 4. Stress–strain curve for cement paste (M0) and graphene–cement paste (GM3).

To study the possible reasons for the increase in compressive strength and the improvement in ductile behavior, the morphology of cement based composite was investigated. Figure 5 shows the morphology of the GNP–cement composite at 7 days and 28 days. In FESEM images of GM3 captured at seven days (Figure 5a), needle form of calcium silicate hydrate (CSH), hexagonal plates of portlandite, graphene nano particle can be observed. ESB or backscattered image was used to distinguish the carbon materials. It can be seen in Figure 5b that graphene nanoparticle are completely black. EDX image was further employed to confirm the presence of graphene and hydrated cement products. The EDX of graphene sheets (Figure 5c) for the location indicated in Figure 5a shows maximum carbon content, clearly confirming the presence of graphene. The EDX for the needle shape CSH in Figure 5d for the location marked in Figure 5b show maximum content of oxygen followed by the silicon and carbon. At 28 days, the needle form of CSH transformed into honeycomb structure of CSH as shown in Figure 5e. The backscattered image or ESB of Figure 5e shows that the hydrated products grow over graphene (Figure 5f). EDX was also employed in Figure 5g,h to confirm the presence of graphene and honeycombed CSH structure. Hence, based on the above information, it can be deduced that, due to the addition of graphene, hydrated products grow in uniform and ordered way [38], which significantly improved the ductile behavior and compressive strength.

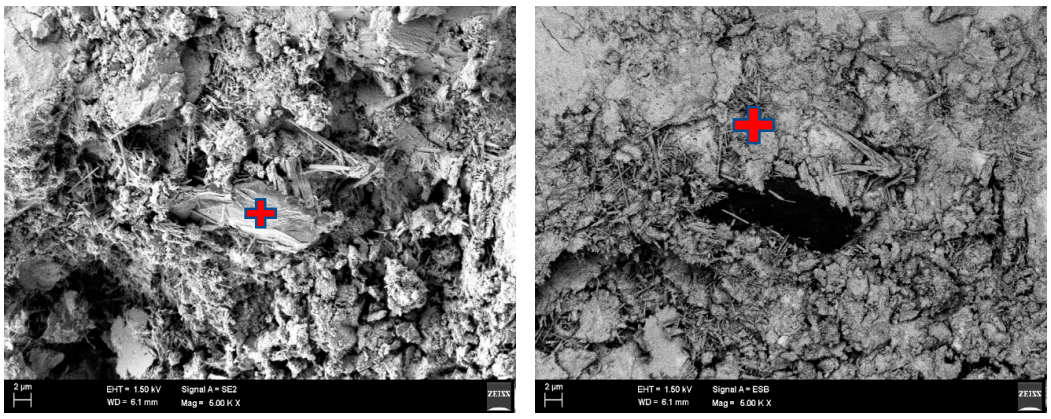

(**a**) (**b**)

Figure 5. *Cont.*

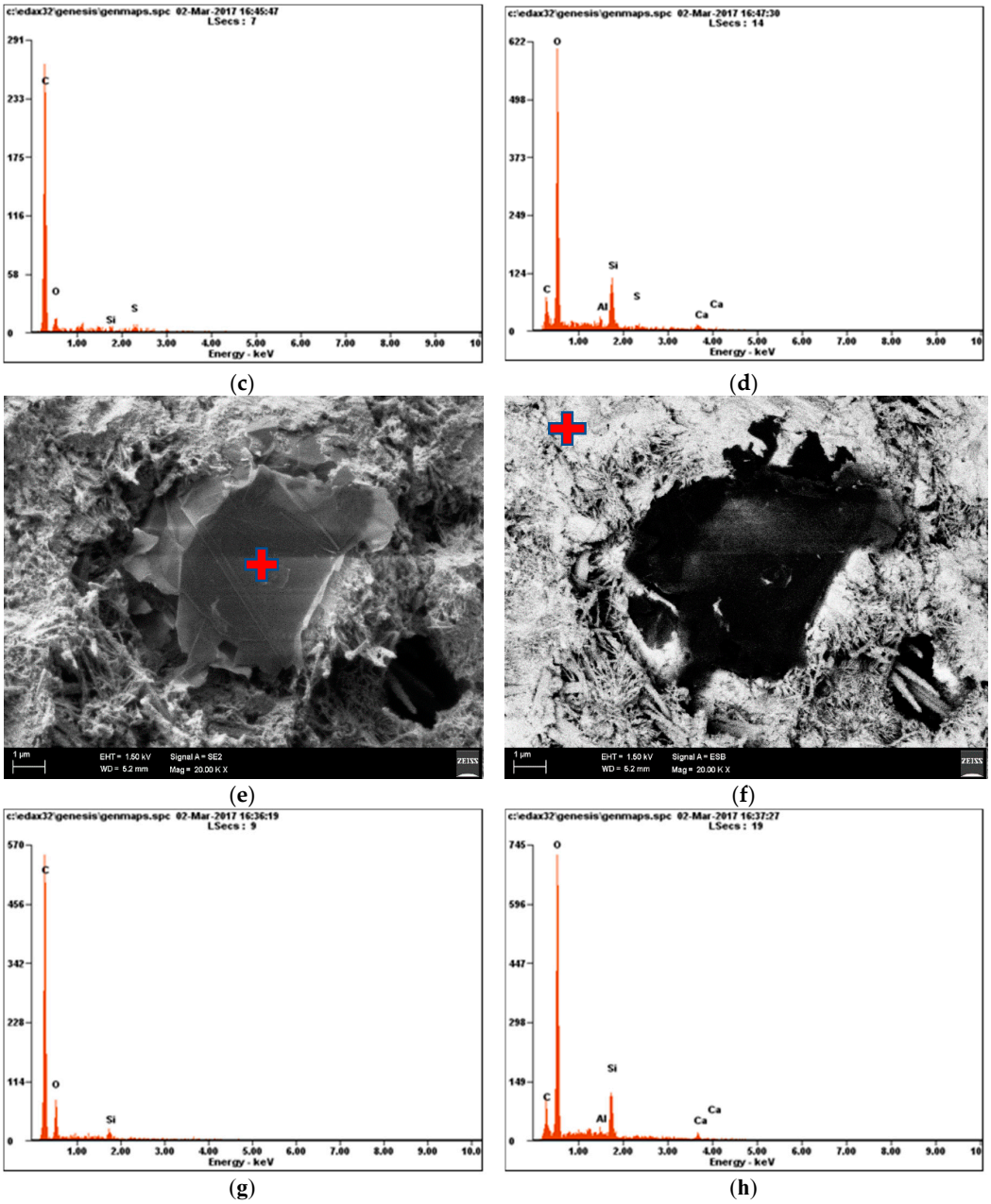

Figure 5. FESEM images of GNP–cement paste at seven days and 28 days: (**a**) FESEM image of GM3 at seven days; (**b**) ESB or backscattered image of (**a**); (**c**) EDX of graphene in GM3 specimen on a point indicated in (**a**); (**d**) EDX for the hydrated cement product at cross hair location in (**b**); (**e**) FESEM image of GM3 at 28 days; (**f**) ESB or backscattered image of (**e**); (**g**) EDX for the marked point in (**e**); and (**h**) EDX at cross-hair location in (**f**).

Generation and growth of cracks for M0 sample were identified using FESEM images, as shown in Figure 6a. These are the nano size cracks; later, due to externally applied forces, they become micro size cracks without any interference and play their role in failure mechanism of material. It can be seen in Figure 6b that graphene successfully interrupted these cracks at nano level and were discontinuous. This is also verified in Figure 6c,d, which shows that graphene platelets are not only holding the micro cracks but are preventing their further growth. Longitudinal growth of cracks is highlighted using green lines while the location of graphene in encircled in red color in Figure 6d. Due to these reasons, the GM3 sample showed more ductile behavior as compared to M0 mix. Pan et al. [36] made the

comparison of crack patterns for plain and graphene oxide based cement composite. The authors found that in plain cement matrix cracks passed straight through the dense hydrated product. However, in graphene oxide cement paste, cracks were fine and discontinued. Therefore, it can be deduced that the presence of graphene sheets would make the cracks fine, the crack pattern discontinuous and provide hindrance to their growth, which, in turn, would result in enhancing the ductility and compressive strength of the graphene cement composite.

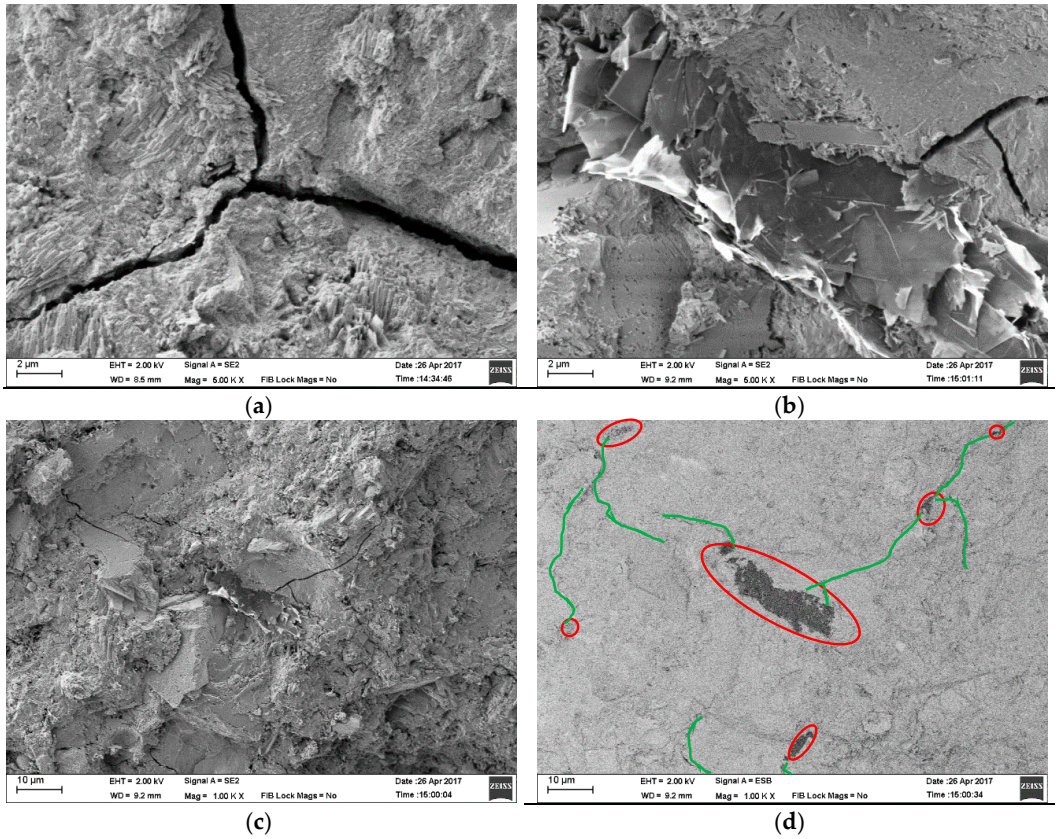

Figure 6. Effect of graphene on propagation of cracks (**a**) Crack propagation in control specimen; (**b**) blockage of the cracks by graphene; (**c**) crack bridging phenomena by graphene; and (**d**) backscattered electron image to identify the graphene in paste.

4.3. Electrical Resistivity Values of the GNP–Cement Composite

Piezo-resistive properties of the M0 and GM3 samples were investigated using the four-probe method. Electrical resistivity for unequal spacing between the probes was calculated using Equation (6).

$$\rho = \frac{V}{I} \times 2\pi \times \frac{1}{\left(\frac{1}{S1} + \frac{1}{S3} - \frac{1}{S1+S2} - \frac{1}{S2+S3}\right)} \quad (6)$$

where V is the floating potential difference between inner two probes, I is current measured by outer two probes, ρ is the resistivity in ohm-cm and S is the spacing in cm and was calculated from current carrying probe to voltage measuring probe. S1 = S3 = 40 cm and S2 = 60 cm.

The results of electrical resistivity are presented in Table 7. The electrical resistivity value at maximum compressive load for GM3 sample was found to be 42% less as compared to M0. To observe the sensing ability of the specimens, normalized compressive loading (NCL) values were calculated. It is the ratio between the applied loads to the maximum compressive load before specimen failure. For

electrical resistance values, the fractional change in resistance (FCR) was used. Equations (7) and (8) present the calculation procedure for the NCL and FCR values.

$$\text{NCL} = \frac{\text{P}}{\text{P}_{\text{max}}} \tag{7}$$

$$\text{FCR} = \frac{\rho_t - \rho_o}{\rho_o} \times 100\% \tag{8}$$

where ρ_t is the electrical resistivity at the given time during the test; ρ_o is the electrical resistivity at the start of the test; P is the compressive loading at the given time during the test; and P_{max} is the maximum compressive loading for the specimen.

Figure 7 shows the fractional change in resistance (in percentage) for M0 and GM3 against the normalized compressive load. It can be seen that in M0 sample the fractional change in resistance is very less as compared to GM3. The results are in line with Li et al. [39]. As graphene is expensive, therefore, it would be very costly to use GNP–cement composite material in a mega project. However, because of superior self-sensing properties, it can be used as a substitute to do health monitoring of the structure. In order to strengthen this view point and show its practical application, full length RC beam was tested in the laboratory by placing GM3 specimen at the time of casting as shown in Figure 2. This beam was subjected to flexural loading and, due to applied loading, cracks were generated in the region of maximum bending moment. Figure 8 shows the fractional change in resistance of GM3 specimen in RC beam. It can be seen that FCR values were varied with the increase in the applied loading on the beam and a sharp response was noted at the time of beam failure. As the beam was subjected to the flexural loading, resistance values were positive. The in-set figure (enlarged view) shows that with the increase in flexural loading, the fractional change in resistance values are also increasing. It is important to mention here that this response in not linear, however, due to the occurrence of damage and propagation of cracks, the FCR values varied as shown in in-set figure (enlarged view of Figure 8). A sudden drop in electrical resistivity value was observed at 22 kN load. The possible reason may be the occurrence of tensile cracks. Initially, tensile cracks started to occur and electrical resistivity values increased linearly. Thereafter, the steel reinforcement started to carry stresses and the significant variation in resistance was noted in GM3 specimen. This effect was more significant as the specimen (GNP cement based composite) was placed in the tensile region, i.e., just above the reinforcement bars. Finally, at the failure stage abrupt increase in FCR was observed, which shows that widening and irreversible crack opening has occurred inside the beam. Hence, structural member is not capable of carrying additional load.

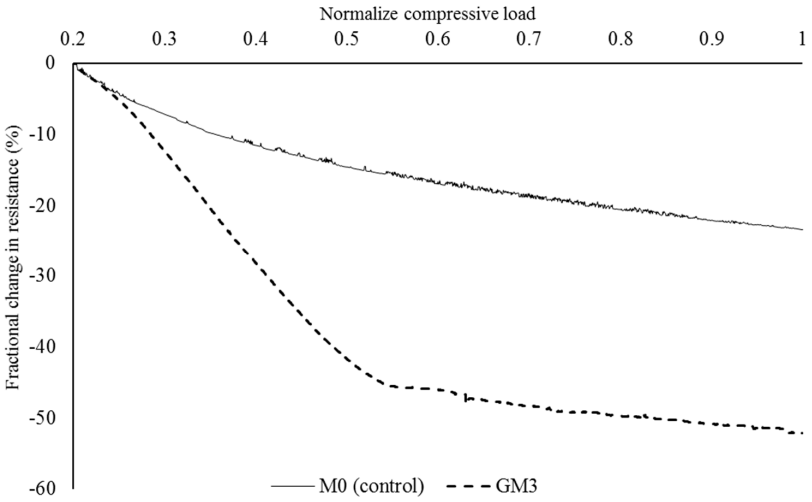

Figure 7. Fractional change in resistance against normalized compression load.

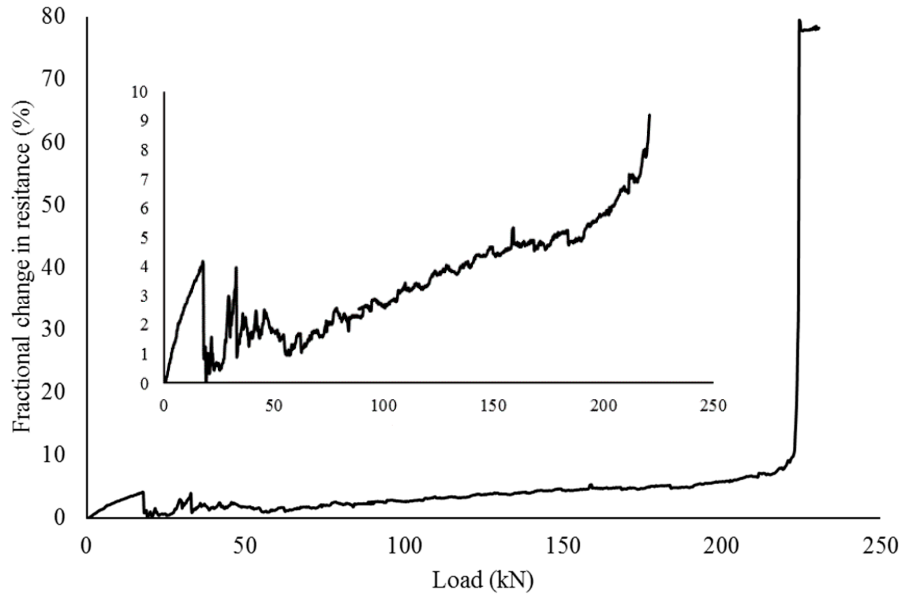

Figure 8. Fractional change in resistance of GM3 specimen against applied compressive loading on the RC beam.

A comparison of strain produced strain against the applied load in reinforcement bars and graphene–cement composite sample is shown in Figure 9. In reinforcement bars, the strain increased linearly and slight variation was observed from 60 kN to 100 kN load as shown in Figure 9a. This variation is very minute and can be neglected for the reinforcement as steel bar was in the linear and elastic region. The GM3 sample also showed variation in strain from 60 kN to 100 kN load as marked in Figure 9a. However, in comparison to reinforcement bar, the variation was large and the strain values for the GM3 sample decreased significantly. This may be related to the redistribution of stresses in the RC concrete beam. Similarly, when the applied loading exceeded 200 kN, the reinforcement bar showed significant variance in strain values. At the same point, an increase in strain values in graphene cement composite sample was noted. It may be related to crushing of concrete in RC concrete beam It is pertinent to mention here that the cost of 5 g of GNPs as per Graphene Laboratories, Inc. USA is 50 USD and 25 cement based composite samples can be casted with GM3 specimen. Hence, GM3 specimen can be used in an efficient and economical way to predict the damages in concrete structures.

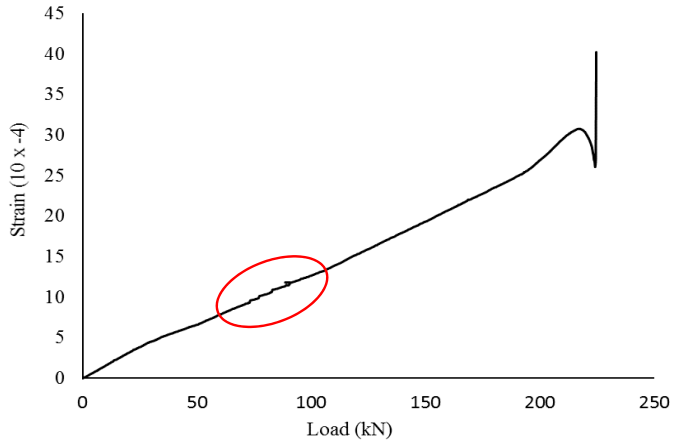

(a)

Figure 9. *Cont.*

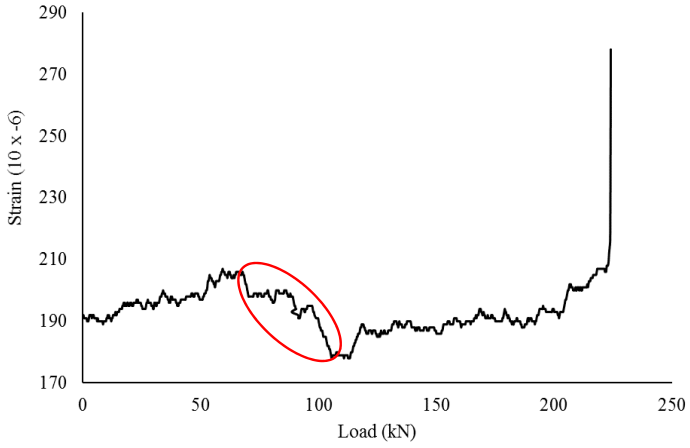

(**b**)

Figure 9. Strain produced by applied compressive load in: (**a**) reinforcement; and (**b**) GNP–cement composite specimen.

5. Conclusions

In this research, cement pastes with different graphene/cement ratio were prepared. Their rheological characteristics of the paste samples were determined from the flow curves of paste using a variety of rheological models, and attained values were analyzed and discussed. After that, hardened properties of the paste were investigated and discussed. Piezo-resistive characteristics of the graphene cement composite were also explored and its practical application was investigated in the laboratory. The following are the conclusions of this research:

1. Generally, for all mixes, the yield stress values estimated by modified Bingham model were the highest while the lowest yield stress values were predicted by Casson model. For all models, the values of yield stress increased with the increase in the content of GNP in cement based composite as well as resting time. For higher shear rate cycle, the yield stress values decreased.
2. For graphene based mixes, Modified Bingham model predicted the higher values of plastic viscosities, while, for control cement paste, Bingham model estimated higher values of plastic viscosities. In general, the plastic viscosities increased with the increase in the content of graphene in the mix and resting time. Reduction in plastic viscosities was observed for higher shear rate cycle.
3. The Standard error resulting from fitting experimental flow curves to various rheological models varied with the content of GNP in cement based composite, shear rate and resting time. Generally, Modified Bingham model best fitted the experimental flow curves while Casson model showed the higher standard error values.
4. Incorporation of GNP showed strong influence on the hardened properties of the cement paste. In comparison to control sample, the GNP cement based composite showed 30% increase in load carrying capacity and 73% increase in overall failure strain.
5. Four-probe method was used to determine the piezo-resistive characteristics of the graphene–cement composite specimen. At maximum compressive load, the electrical resistivity value reduced by 42%. From the results of fractional change in resistance, it can be concluded that GNP cement based composite can be used to detect the damages in concrete.
6. Practical application of graphene–cement composite specimen was evaluated on RC beam. It was found that electrical resistance values varied with the increase in the applied load. Moreover, the graphene–cement composite specimen successfully predicted the response against crack propagation.

Based on above findings, graphene cement composite provides an economical and efficient solution for monitoring the structural health of the concrete members throughout their life span.

Acknowledgments: This research was supported by University Malaya Research Grant (UMRG-Project No. RP004A/13AET), University Malaya Postgraduate Research Fund (PPP-Project No. PG217–2014B) and Fundamental Research Grant Scheme, Ministry of Education, Malaysia (FRGS-Project No. FP004–2014B).

Author Contributions: Sardar Kashif Ur Rehman and Zainah Ibrahim conceived and designed the experiments; Muhammad Faisal Javed and Sardar Kashif Ur Rehman performed the experiments; Sardar Kashif Ur Rehman and Shazim Ali Memon analyzed the data; Zainah Ibrahim contributed reagents/materials/analysis tools; and Sardar Kashif Ur Rehman, Rao Arsalan Khushnood and Shazim Ali Memon wrote the paper.

Conflicts of Interest: The authors declare no conflict of interest.

References

1. Zhang, Y.; Kong, X.; Gao, L.; Lu, Z.; Zhou, S.; Dong, B. In-situ measurement of viscoelastic properties of fresh cement paste by a microrheology analyzer. *Cem. Concr. Res.* **2016**, *79*, 291–300. [CrossRef]
2. Ferraris, C.F. Measurement of the rheological properties of cement paste: A new approach. In *International RILEM Conference on the Role of Admixtures in High Performance Concrete*; National Institute of Standards and Technology: Gaithersburg, MD, USA, 1999; pp. 333–342.
3. Kawashima, S.; Hou, P.; Corr, D.J.; Shah, S.P. Modification of cement-based materials with nanoparticles. *Cem. Concr. Compos.* **2013**, *36*, 8–15. [CrossRef]
4. Ormsby, R.; McNally, T.; Mitchell, C.; Halley, P.; Martin, D.; Nicholson, T. Effect of MWCNT addition on the thermal and rheological properties of polymethyl methacrylate bone cement. *Carbon* **2011**, *49*, 2893–2904. [CrossRef]
5. Konsta-Gdoutos, M.S.; Metaxa, Z.S.; Shah, S.P. Highly dispersed carbon nanotube reinforced cement based materials. *Cem. Concr. Res.* **2010**, *40*, 1052–1059. [CrossRef]
6. Shang, Y.; Zhang, D.; Yang, C.; Liu, Y.; Liu, Y. Effect of graphene oxide on the rheological properties of cement pastes. *Constr. Build. Mater.* **2015**, *96*, 20–28. [CrossRef]
7. Wang, Q.; Wang, J.; Lv, C.-X.; Cui, X.-Y.; Li, S.-Y.; Wang, X. Rheological behavior of fresh cement pastes with a graphene oxide additive. *New Carbon Mater.* **2016**, *31*, 574–584. [CrossRef]
8. Wang, Q.; Cui, X.; Wang, J.; Li, S.; Lv, C.; Dong, Y. Effect of fly ash on rheological properties of graphene oxide cement paste. *Constr. Build. Mater.* **2017**, *138*, 35–44. [CrossRef]
9. Nehdi, M.; Rahman, M.A. Estimating rheological properties of cement pastes using various rheological models for different test geometry, gap and surface friction. *Cem. Concr. Res.* **2004**, *34*, 1993–2007. [CrossRef]
10. Lee, C.; Wei, X.; Kysar, J.W.; Hone, J. Measurement of the elastic properties and intrinsic strength of monolayer graphene. *Science* **2008**, *321*, 385–388. [CrossRef] [PubMed]
11. Rehman, S.K.U.; Ibrahim, Z.; Memon, S.A.; Jameel, M. Nondestructive test methods for concrete bridges: A review. *Constr. Build. Mater.* **2016**, *107*, 58–86. [CrossRef]
12. Chung, D. Piezoresistive cement-based materials for strain sensing. *J. Intell. Mater. Syst. Struct.* **2002**, *13*, 599–609. [CrossRef]
13. Sanchez, F.; Sobolev, K. Nanotechnology in concrete—A review. *Constr. Build. Mater.* **2010**, *24*, 2060–2071. [CrossRef]
14. Raki, L.; Beaudoin, J.; Alizadeh, R.; Makar, J.; Sato, T. Cement and concrete nanoscience and nanotechnology. *Materials* **2010**, *3*, 918–942. [CrossRef]
15. Sobolev, K.; Gutiérrez, M.F. How nanotechnology can change the concrete world. *Am. Ceram. Soci. Bull.* **2005**, *84*, 14.
16. Mukhopadhyay, A.K. Next-generation nano-based concrete construction products: A review. In *Nanotechnology in Civil Infrastructure*; Springer: Berlin/Heidelberg, Germany, 2011; pp. 207–223.
17. Vajtai, R. *Springer Handbook of Nanomaterials: Springer Science & Business Media*; Springer: Berlin/Heidelberg, Germany, 2013.
18. Sixuan, H. Multifunctional Graphite Nanoplatelets (GNP) Reinforced Cementitious Composites. Ph.D. Thesis, Tsinghua University, Beijing, China, 2012.
19. Papo, A. Rheological models for cement pastes. *Mater. Struct.* **1988**, *21*, 41–46. [CrossRef]

20. Yahia, A.; Khayat, K.H. Analytical models for estimating yield stress of high-performance pseudoplastic grout. *Cem. Concr. Res.* **2001**, *31*, 731–738. [CrossRef]
21. Rao, M.A. Flow and functional models for rheological properties of fluid foods. In *Rheology of Fluid, Semisolid, and Solid Foods*; Springer: Berlin/Heidelberg, Germany, 2014; pp. 27–61.
22. Yahia, A.; Khayat, K. Applicability of rheological models to high-performance grouts containing supplementary cementitious materials and viscosity enhancing admixture. *Mater. Struct.* **2003**, *36*, 402–412. [CrossRef]
23. Scott Blair, G. The success of Casson's equation. *Rheol. Acta* **1966**, *5*, 184–187. [CrossRef]
24. American Society for Testing and Materials. *Standard Test Method for Flow of Hydraulic Cement Mortar*; ASTM International: West Conshohocken, PA, USA, 2015.
25. Roussel, N.; Ovarlez, G.; Garrault, S.; Brumaud, C. The origins of thixotropy of fresh cement pastes. *Cem. Concr. Res.* **2012**, *42*, 148–157. [CrossRef]
26. Han, B.G.; Han, B.Z.; Ou, J.P. Experimental study on use of nickel powder-filled Portland cement-based composite for fabrication of piezoresistive sensors with high sensitivity. *Sens. Actuators A Phys.* **2009**, *149*, 51–55. [CrossRef]
27. Han, B.; Guan, X.; Ou, J. Electrode design, measuring method and data acquisition system of carbon fiber cement paste piezoresistive sensors. *Sens. Actuators A Phys.* **2007**, *135*, 360–369. [CrossRef]
28. Li, G.Y.; Wang, P.M.; Zhao, X. Pressure-sensitive properties and microstructure of carbon nanotube reinforced cement composites. *Cem. Concr. Compos.* **2007**, *29*, 377–382. [CrossRef]
29. Le, J.-L.; Du, H.; Dai Pang, S. Use of 2D Graphene Nanoplatelets (GNP) in cement composites for structural health evaluation. *Compos. Part B Eng.* **2014**, *67*, 555–563.
30. Dai Pang, S.; Gao, H.J.; Xu, C.; Quek, S.T.; Du, H. Strain and damage self-sensing cement composites with conductive graphene nanoplatelet. In *SPIE Smart Structures and Materials+ Nondestructive Evaluation and Health Monitoring*; International Society for Optics and Photonics; SPIE: San Diego, CA, USA, 2014; p. 906126.
31. Shaughnessy, R.; Clark, P.E. The rheological behavior of fresh cement pastes. *Cem. Concr. Res.* **1988**, *18*, 327–341. [CrossRef]
32. Barnes, H.A. A handbook of elementary rheology. In *Institute of Non-Newtonian Fluid Mechanics*; University of Wales: Wales, UK, First published 2000; ISBN 0-9538032-0-1.
33. Chuah, S.; Pan, Z.; Sanjayan, J.G.; Wang, C.M.; Duan, W.H. Nano reinforced cement and concrete composites and new perspective from graphene oxide. *Constr. Build. Mater.* **2014**, *73*, 113–124. [CrossRef]
34. Vikan, H.; Justnes, H.; Winnefeld, F.; Figi, R. Correlating cement characteristics with rheology of paste. *Cem. Concr. Res.* **2007**, *37*, 1502–1511. [CrossRef]
35. Wallevik, J.E. Rheological properties of cement paste: Thixotropic behavior and structural breakdown. *Cem. Concr. Res.* **2009**, *39*, 14–29. [CrossRef]
36. Pan, Z.; He, L.; Qiu, L.; Korayem, A.H.; Li, G.; Zhu, J.W. Mechanical properties and microstructure of a graphene oxide–cement composite. *Cem. Concr. Compos.* **2015**, *58*, 140–147. [CrossRef]
37. Collins, F.; Lambert, J.; Duan, W.H. The influences of admixtures on the dispersion, workability, and strength of carbon nanotube–OPC paste mixtures. *Cem. Concr. Compos.* **2012**, *34*, 201–207. [CrossRef]
38. Cao, M.-L.; Zhang, H.-X.; Zhang, C. Effect of graphene on mechanical properties of cement mortars. *J. Cent. South Univ.* **2016**, *23*, 919–925. [CrossRef]
39. Li, H.; Xiao, H.-G.; Ou, J.-P. A study on mechanical and pressure-sensitive properties of cement mortar with nanophase materials. *Cem. Concr. Res.* **2004**, *34*, 435–438. [CrossRef]